Minireview

Quantitative optical coherence tomography angiography: A review

Xincheng Yao[1,2], Minhaj N Alam[1], David Le[1] and Devrim Toslak[1,3]

[1]Department of Bioengineering, University of Illinois at Chicago, Chicago, IL 60607, USA; [2]Department of Ophthalmology and Visual Sciences, University of Illinois at Chicago, Chicago, IL 60612, USA; [3]Department of Ophthalmology, Antalya Training and Research Hospital, Antalya 07030, Turkey

Corresponding author: Xincheng Yao. Email: xcy@uic.edu

Impact statement

OCT angiography (OCTA) provides a noninvasive method to detect microvascular distortions correlated with eye conditions. Quantitative analysis of OCTA is essential to standardize objective interpretations of clinical outcome. This review summarizes technical rationales and clinical applications of quantitative OCTA features.

Abstract

As a new optical coherence tomography (OCT) modality, OCT angiography (OCTA) provides a noninvasive method to detect microvascular distortions correlated with eye conditions. By providing unparalleled capability to differentiate individual plexus layers in the retina, OCTA has demonstrated its excellence in clinical management of diabetic retinopathy, glaucoma, sickle cell retinopathy, diabetic macular edema, and other eye diseases. Quantitative OCTA analysis of retinal and choroidal vasculatures is essential to standardize objective interpretations of clinical outcome. Quantitative features, including blood vessel tortuosity, blood vessel caliber, blood vessel density, vessel perimeter index, fovea avascular zone area, fovea avascular zone contour irregularity, vessel branching coefficient, vessel branching angle, branching width ratio, and choroidal vascular analysis have been established for objective OCTA assessment. Moreover, differential artery–vein analysis has been recently demonstrated to improve OCTA performance for objective detection and classification of eye diseases. In this review, technical rationales and clinical applications of these quantitative OCTA features are summarized, and future prospects for using these quantitative OCTA features for artificial intelligence classification of eye conditions are discussed.

Keywords: Optical coherence tomography angiography, quantitative analysis, retinopathy, eye condition, eye disease, diabetic retinopathy, sickle cell retinopathy, classification

***Experimental Biology and Medicine* 2020; 245: 301–312. DOI: 10.1177/1535370219899893**

Introduction

As one part of the central nervous system, the retina is a neurovascular complex network located at the back of the eye. Color fundus photography has provided valuable information for eye disease detection and treatment assessment, but the spatial resolution and image contrast are limited to reveal subtle distortions in early stages of eye diseases. Scanning laser ophthalmoscopy[1,2] and adaptive optics[3–5] imaging systems provide enhanced image resolution, and fundus angiography[6,7] allows better contrast of retinal vasculatures. However, these imaging approaches lack sectioning capability to differentiate individual retinal neural layers and vascular plexuses. It is known that different diseases and stages can target retinal neurons and vasculatures in different ways. Given the unprecedented capability to differentiate individual functional layers, optical coherence tomography (OCT)[8] has been extensively employed for depth-resolved examination of morphological abnormalities caused by eye diseases.[9–11]

As a new OCT modality, OCT angiography (OCTA) provides a noninvasive method to differentiate individual plexus layers in the retina.[12,13] Since its first commercial product in 2014, OCTA has quickly demonstrated its excellence in clinical management of diabetic retinopathy (DR),[14,15] glaucoma,[16,17] sickle cell retinopathy (SCR),[18] age-related macular degeneration (AMD),[19] and other eye diseases. Quantitative OCTA analysis is essential to standardize objective interpretation of clinical outcomes.

Multiple OCTA features have been recently developed for quantitative analysis of vascular distortions due to eye conditions. In the following sections, technical rationales of these quantitative OCTA features will be summarized. Current status and future prospects of using OCTA features for objective detection and artificial intelligence (AI) classification of eye diseases will be discussed.

Quantitative OCTA features

In this section, technical rationale of OCTA features, i.e. blood vessel tortuosity (BVT), blood vessel caliber (BVC), blood vessel density (BVD), vessel perimeter index (VPI), fovea avascular zone area (FAZ-A), FAZ contour irregularity (FAZ-CI), vessel complexity index (VCI), branchpoint analysis (BPA), differential artery–vein (A–V) analysis, flow analysis, and choroidal neurovasculature (CNV) analysis will be explained sequentially. To help the explanation of quantitative OCTA analysis, Figure 1 illustrates major procedures of quantitative feature extraction.

BVD

BVD, also named as vessel density (VD),[21] vessel area density,[22] capillary density,[23] or percent area of non-perfusion,[24] reflects the ratio of the image area occupied by the blood vessels (Figure 1(b)). Eye diseases such as DR,[25,26] SCR,[27,28] AMD,[29,30] glaucoma,[31,32] and vein occlusion (VO)[33,34] may involve vessel abnormalities, including ischemia and drop out zones in retinal and choroidal vasculatures. Most of these diseases manifest at the capillary level at early phases, which can be detected in OCTA. BVD can be quantified as[35]

$$BVD = \frac{\sum_{x=1,\ y=1}^{n} A(x,y)}{\sum_{x=1,y=1}^{n} I(x,y)} \tag{1}$$

where $A(x,y)$ represents the pixels occupied by the vessels, and $I(x,y)$ represents all the pixels in the OCTA image. In this article, the OCTA image is assumed to be a square frame, consisting of $n \times n$ pixels, and x and y correspond to the horizontal and vertical coordinates of individual pixels.

If the skeletonized vessel map (Figure 1(c)) is used for VD analysis, this feature is alternatively termed as vessel skeleton density (VSD) or skeleton density.[32] The VSD can be quantified as[36]

$$VSD = \frac{\sum_{x=1,\ y=1}^{n} S(x,y)}{\sum_{x=1,y=1}^{n} I(x,y)} \tag{2}$$

where $S(x,y)$ represents the pixels occupied by the vessel skeleton and $I(x,y)$ represents all the pixels in the OCTA.

BVC

BVC, also named as vessel diameter, vessel width, or vessel diameter index,[37] is used to quantify vascular dilation or shrinkage due to eye conditions. BVC distortions have been commonly observed in different retinopathies, such as SCR[35,38] and DR.[39] The BVC can be calculated as the ratio of the vessel area to the vessel length[35]

$$BVC = \frac{\sum_{x=1,\ y=1}^{n} A(x,y)}{\sum_{x=1,y=1}^{n} S(x,y)} \tag{3}$$

where $A(x,y)$ represents the pixels occupied by the vessels in the segmented vessel map (Figure 1(b)) and $S(x,y)$ represents the pixels occupied by the vessels in the skeletonized vessel map (Figure 1(c)). In the skeletonized map, the width of each vessel is one pixel. Therefore, $\sum_{x=1,\ y=1}^{n} A(x,y)$ represents total vessel area, and $\sum_{x=1,y=1}^{n} S(x,y)$ represents overall vessel length.

BVT

BVT[35,38] is a measure of the degree of vessel distortion. In normal condition, the blood vessels transport blood efficiently, with a relatively smooth structure. However, in diseased conditions,[35,38–41] the transportation efficiency of some blood vessels may be compromised due to distorted structure. The tortuosity of each blood vessel can be quantified by measuring the ratio of the geodesic distance to the Euclidean distance[35]

$$BVT = \frac{1}{n}\sum_{i=1}^{n}\left(\frac{\left\{\begin{array}{c}Geodesic\ distance\ between\ two\\ endpoints\ of\ a\ vessel\ branch\ i\end{array}\right\}}{\left\{\begin{array}{c}Euclidean\ distance\ between\ two\\ endpoints\ of\ a\ vessel\ branch\ i\end{array}\right\}}\right) \tag{4}$$

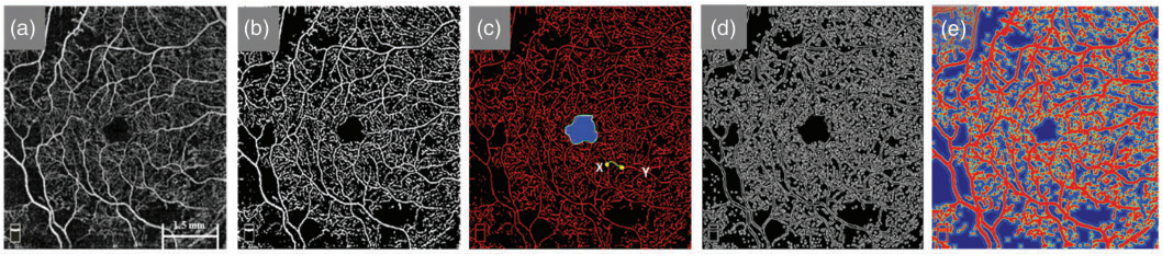

Figure 1. Feature extraction for quantitative OCTA analysis. (a) Representative OCTA image from a DR patient. (b) Segmented blood vessel map. (c) Skeletonized blood vessel map (red) with segmented fovea (blue region) and FAZ contour (green curve). One representative vessel branch is highlighted in green with X and Y endpoints identified with yellow dots. (d) Vessel perimeter map. (e) FD contour map. Source: Modified from Alam *et al.*[20] (A color version of this figure is available in the online journal.)

where i represents the ith branch and n is the total number of branches; Euclidian distance is the straight-line distance between two end points of a vessel branch and geodesic distance is the total curve length between two end points (shown in Figure 1(c)).

VPI

VPI[42] measures the ratio between overall contour length of blood vessel boundaries (Figure 1(d)) and total blood vessel area in the segmented vessel map (Figure 1(b)). VPI can reflect vessel dropout or early ischemia,[39,43] and has been used to quantify OCTA images of DR[43] and SCR.[38] It can be measured as follows[35]

$$VPI = \frac{\sum_{x=1,\ y=1}^{n} P(x,y)}{\sum_{x=1,y=1}^{n} I(x,y)} \tag{5}$$

where $P(x,y)$ represents the pixels within the vessel perimeters, i.e. the overall contour length of blood vessel boundaries (Figure 1(d)), and $I(x,y)$ represents all the pixels occupied by the blood vessels, i.e. total blood vessel area (Figure 1(b)).

FAZ

Foveal shape can be affected by eye diseases such as DR,[44] SCR,[38] and VO,[45] due to parafoveal vessel drop out and foveal ischemia. FAZ-A has been demonstrated as a sensitive feature to differentiate severities of non-proliferative diabetic retinopathy (NPDR).[39] The FAZ-A is measured by segmenting the FAZ (demarcated as a blue region in Figure 1(c)) and calculating the total area using the following equation[35]

$$FAZ - A = \left[Area\ of\ single\ pixel\ (in\ \mu m^2) \times \sum_{x=1,\ y=1}^{n} A(x,y) \right] \tag{6}$$

where $A(x,y)$ represents the pixels occupied by the segmented FAZ region.

FAZ-CI

FAZ-CI, also named as FAZ-circularity[38] or FAZ acircularity index,[46] measures the structural irregularity of the foveal shape.[38] FAZ-CI distortions have been observed in DR,[46] AMD,[47] SCR,[35] and glaucoma.[48] The FAZ-CI can be quantified by calculating the ratio of the perimeter of the FAZ-A to the perimeter of a reference circle with area identical to the FAZ[35]

$$FAZ - CI = \frac{\sum_{x=1,\ y=1}^{n1} O(x,y)}{\sum_{x=1,y=1}^{n2} R(x,y)} \tag{7}$$

where $O(x,y)$ represents the pixels occupied by the perimeter of the FAZ (green demarcation in Figure 1(c)), $R(x,y)$ represents the pixels occupied by the perimeter of a reference circle with area identical to the segmented FAZ, $n1$ denotes the maximum number of pixels that encompasses the perimeter of the FAZ, $n2$ denotes the maximum number of pixels that encompasses the perimeter of the reference circle, x and y denote the pixel coordinates with respect to the perimeter of the FAZ or reference circle.

VCI

Fractal dimension (FD) has been used as a parameter to quantify the VCI (Figure 1(e)). FD is commonly calculated with the box-counting method in which a relationship is established by the number of boxes (of a certain resolution) that enclose the pattern in an image (Figure 1(e)).[49] This count is iteratively measured for different image scales. The box-counting method is formalized as[49]

$$FD = \frac{\log N_r}{\log r^{-1}} \tag{8}$$

where N_r is the number of boxes that encloses the pattern by the scale of the image, r. Lacunarity (LAC) is a complementary parameter to FD and is a measure of rotational inhomogeneity or the voids between vessel structures.[50] LAC provides information regarding the distribution and size of gaps in a binary image and is calculated using a similar box-counting strategy as the FD.

BPA

It is well known that decreased efficiency in blood transport can affect bifurcation in vascular structures.[51] Quantitative BPA, including both angle and width features (Figure 2), has been recently demonstrated for objective OCTA classification of DR.[52] For angle parameters, vessel branching angle and child (also referred to as daughter) branching angles (CBA1 and CBA2) are measured to quantify changes in bifurcation.[52] As shown in Figure 2, in order to determine the branching angles, the branchpoint (green dots, Figure 2(b)) must first be determined, and then the vessel endpoints (red dots, Figure 2(c)). For the application in Figure 2, a radius of 0.097 mm was empirically determined and used to identify the vessel endpoints. It should be noted that there are no strict guidelines; however, the user should choose a radius that is large enough to contain the region of interest and small enough to not overlap with adjacent branchpoints. Furthermore, the application was for a 6×6 mm^2 FOV, therefore for other FOV, i.e. 3×3 mm^2 or 8×8 mm^2, the user should adjust accordingly. After identification of the vessel endpoints, using geometric identities the branchpoint angles, including the overall branching angle θ, and the individual child angles $\alpha 1$ and $\alpha 2$ (Figure 2(d)), are determined. Furthermore, an area of approximately 0.157×0.157 mm^2 surrounding the vessel endpoints was used to determine the width of each vessel.[52] Similarly, the area size for width measurement should also be tailored to the specific application.

Utilizing the vessel widths, three width-based parameters were determined, i.e. the vessel branching coefficient

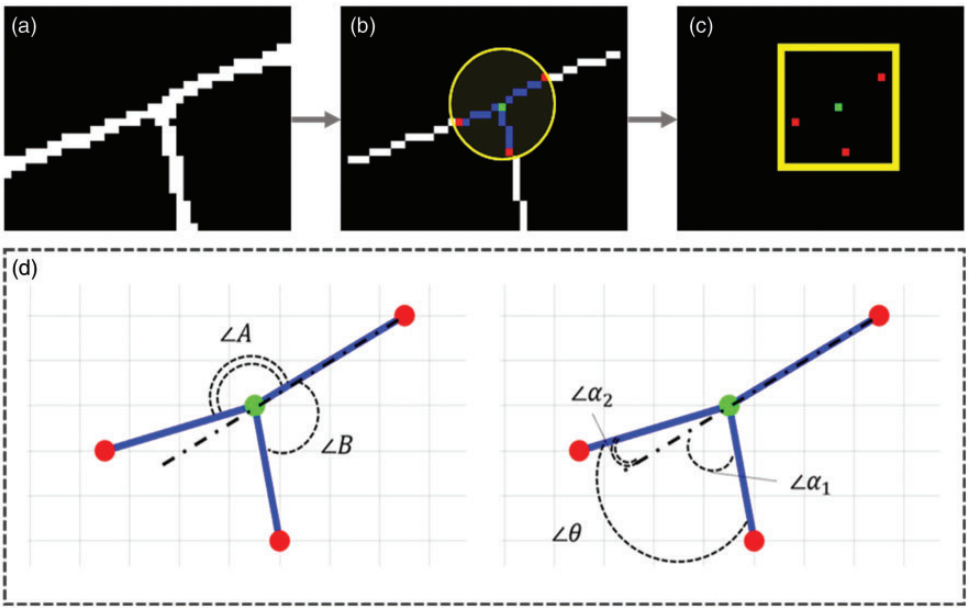

Figure 2. (a) Sample branchpoint. (b) Branchpoint in a vessel skeleton, where the green pixel represents the branchpoint, the red pixels represent the end points, the blue pixels represent our vessels of interest, and the yellow circle represents the dilated area. (c) A composite image of the branchpoint (green) and endpoint (red), where the yellow square represents the window area. (D) Branch angle measurement. Angles A and B in the left image are complementary angles used to calculate θ, $\alpha 1$, and $\alpha 2$ in the right image. Source: Modified from Le *et al.*[52] (A color version of this figure is available in the online journal.)

and child width ratios are calculated to measure the structural change of the vessels as a result of bifurcation[52]

$$VBC = \frac{d_1^2 + d_2^2}{d_0^2} \tag{9}$$

$$CWR_i = \frac{d_i}{d_0} \tag{10}$$

where d_0 is the width of the parent vessel, d_1 and d_2 are the widths of the child vessels, and i represents the ith child vessel. As noted by Le *et al.*,[52] due to ischemia and neovascularization caused by DR, changes in vessel widths and branching angles could be related to vascular remodeling. We presume that branch geometry could be well correlated with other OCTA features such as BVT or VPI.

Differential A–V analysis

Differential A–V analysis compares the changes in arteries relative to the veins. Color fundus image analysis has been demonstrated to guide A–V classification in OCTA (Figure 3), showing improved sensitivity of OCTA detection of DR[41] and SCR.[35,38] For color fundus image guidance, vessel nodes are identified as arteries and veins by evaluating optical density ratio between red and green channels of the fundus image.[41] Once the source nodes have been identified, a fundus A–V map is generated. Employing image registration for the fundus and corresponding OCTA images, a vessel tracking algorithm is implemented to generate an A–V map in OCTA guided by the fundus A–V map.[41] In addition to the color fundus image guided A–V differentiation in OCTA, OCT feature analysis guided A–V differentiation[53] and near infrared oximetry guided A–V differentiation[54] have been also demonstrated.

Flow analysis

Several parameters, including the flow index (FI),[55] adjusted flow index,[24] flow void (FV),[56] vascular connectivity,[57] and total retinal blood flow (TRBF), have been developed to quantify alterations in blood flow.[58] The information captured by OCTA is the decorrelation value of each pixel. Higher blood flow velocity results in increased decorrelation, i.e. enhanced OCTA brightness. FI is defined as the average decorrelation value within a region of interest in the en-face OCTA.[59] The FI can be measured by using the following equation

$$FI = \frac{\sum_{x=1,\ y=1}^{n} A(x,y)}{N} \tag{11}$$

where $A(x,y)$ represents the decorrelation of the pixel (x,y) and N is total the number of pixels in the OCTA image.

The FV is calculated as the percentage of the area without flow signal over the total scanned region[56]

$$FV = \frac{Area_{Flowvoid}}{Area_{whole}} \times 100\% \tag{12}$$

Because BVD represents the percentage of the area with flow signal over the total scanned region, the FV can also be determined by

$$FV = 1 - BVD \tag{13}$$

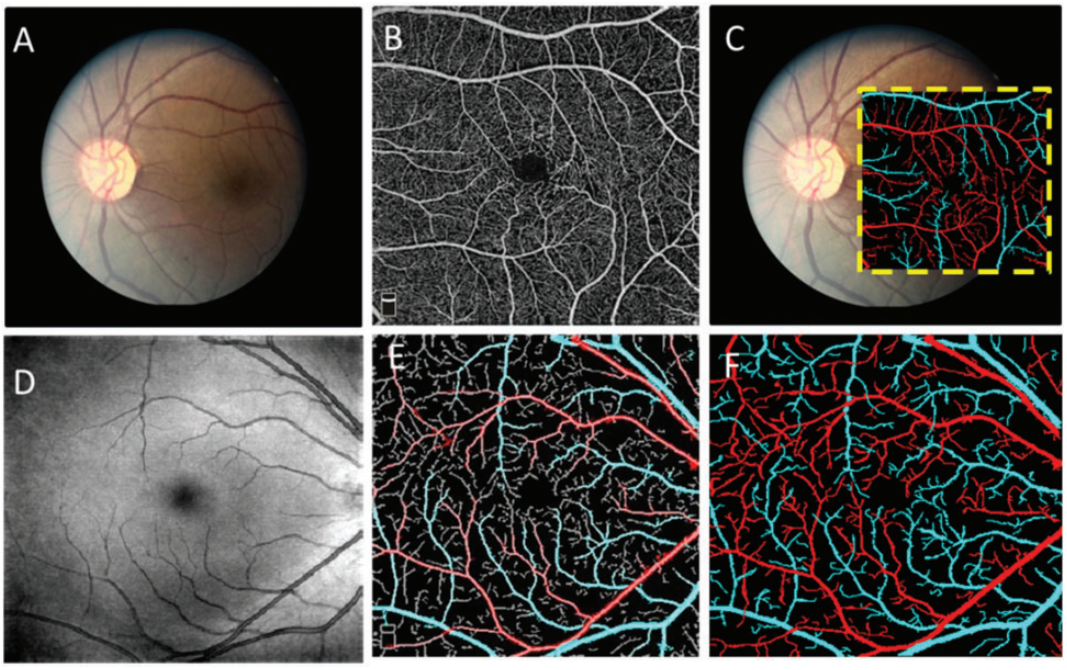

Figure 3. A–V classification using fundus guided (row 1) and en-face OCT guided (row 2) techniques developed by Alam *et al.*[41,53] (a) Sample fundus image, (b) corresponding OCTA image, (c) OCTA A–V map overlaid on the fundus image, (d) sample OCT en-face image, (e) A–V information from en-face OCT overlaid on OCTA binary vessel map, and (f) OCTA A–V map. Source: Modified from Alam *et al.*[41,53] (A color version of this figure is available in the online journal.)

TRBF is a parameter used to estimate the flow of all vessel segments with Doppler OCT. TRBF is determined by integrating the axial velocity derived from the Doppler phase shift in the en-face plane[58]

$$TRBF = -\int\int_{xy-plane} v_z(x,y)\mathrm{d}x\mathrm{d}y \tag{14}$$

where the flow in a vessel is computed by integrating the axial flow velocity $v_z(x,y)$ measured from different pixels in the en-face image over the surface $(xy-plane)$ normal to $v_z(x,y)$.[58] This method is primarily used in OCTA systems with high acquisition speeds, e.g. 100 kHz. For slower acquisition speeds, e.g. 70 kHz, strategies have been developed to determine TRBF using optimized en-face planes.[59,60]

Another important OCTA parameter related to flow was described by variable interscan time analysis (VISTA),[61,62] which was performed to assess the alteration of choriocapillaris and differentiate varying degrees of flow impairment. VISTA has been used to quantify NPDR, PDR, geographic atrophy (GA), and AMD eyes.

CNV analysis

CNV analysis has been used to assess morphological distortions, named as seafan, medusa, tangled, and dead-tree, in choroidal vasculature.[30] A commonly examined parameter is CNV area, which can be determined as follows[63]

$$\begin{aligned} CNV\ area\ (mm^2) = {} & CNV\ area\ (pixel) \\ & \times (3\,mm/304\,pixel)^2 \end{aligned} \tag{15}$$

where 3 mm represents the 3 mm FOV OCTA images (304×304 pixels) used in Uchida *et al.*[63]

The essential step for quantitative OCTA analysis is reliable segmentation of CNV (Figure 4).

The segmentation has been commonly performed using manual or semi-manual processes.[12] Projection-resolved (PR-OCTA) method has been explored to determine the CNV area and skeleton automatically.[57] The binarized vessel or skeleton map of CNV area can be used for FD analysis using Fractalyse and likewise.[30] BVD or LAC can also be determined from the vessel or skeleton map. Other characteristics used to assess CNV include CNV location, CNV maturity, the presence of core vessels, and the presence of margin loops.[64] Quantitative OCTA parameters, such as BVD, FD,[30] and LAC,[65] have also been used for CNV analysis of AMD.[30] They are useful parameters to evaluate neovascularization activity by assessing the degree of complexity, and vessel nonuniformity of the lesions, respectively.

Discussion

Fundus photography has been established for clinical management of eye diseases. However, the spatial resolution and image contrast of traditional color fundus cameras are limited to reveal subtle distortion of retinal and choroidal vasculatures in early stages of eye diseases. OCTA provides a label-free solution for high resolution examination of ocular vasculatures. With depth-resolved capability to visualize retinal vasculatures at capillary level resolution, OCTA has been rapidly adopted for clinical management of eye diseases.

A brief summary of quantitative OCTA features established for clinical and custom OCTA instruments is listed in

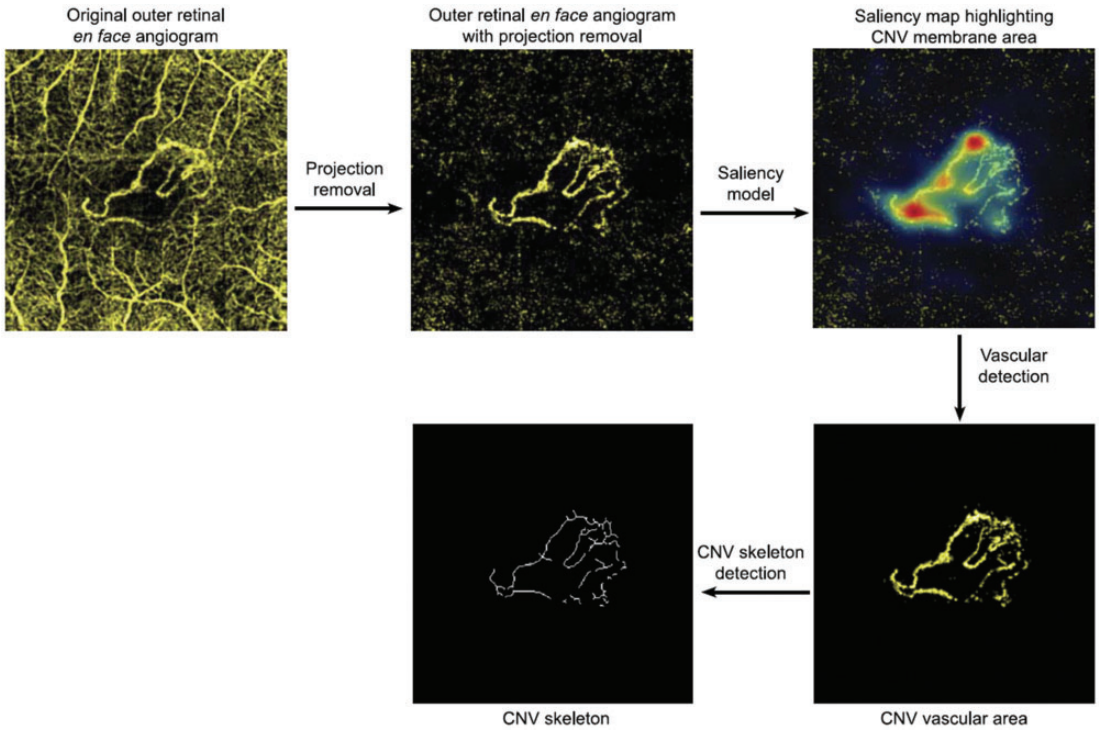

Figure 4. Method of determining CNV area and skeleton. Illustrative steps of generating the CNV area and skeleton from the original outer retinal en-face OCTA image using a saliency model. Source: Reprinted from Patel *et al.*[57](A color version of this figure is available in the online journal.)
CNV: choroidal neovascular.

Table 1 along with demonstrated applications. Quantitative features, including BVT, BVC, BVD, VPI, FAZ-A, FAZ-CI, VCI, BPA, and differential A–V analysis, have been demonstrated to foster the standardization of objective interpretation of OCTA. Pathological mechanisms may affect the OCTA features sensitive to eye conditions. In other words, different eye diseases may cause OCTA distortions in different ways. For example, SCR is known to produce sickle shaped blood cells, which may lead to tortuous and dilated vessels that can be quantified by BVT and BVC, respectively. BVT has been recently demonstrated as the most sensitive feature for SCR detection and classification.[20] DR patients may frequently accompany with hypertension to cause arterial narrowing[41] that can be quantified by BVC analysis. Capillary level ischemia can be assessed by BVD analysis in DR patients.[39] BVD has also been used to evaluate central and branch VOs.[34,45,124,161,162] BVD, FAZ-A, and FAZ-CI have been commonly used for OCTA assessment of glaucoma.[48,78] Recent studies also suggest that vascular distortions may manifest in different regions due to different diseases. For example, localized BVD measurements revealed perifoveal region as the most sensitive region to classify NPDR stages.[39,79] However, for SCR, the parafoveal in the temporal retina was the most sensitive region for SCR staging.[38]

Differential A–V analysis has been demonstrated to improve OCTA performance.[40,41] Pathological alterations in the artery and vein compartments are known to be affected in different ways.[163] For example, DR may cause increased arterial tortuosity, venous beading, narrowing artery, and dilated vein.[164] If only mean value of arterial and venous distortions is evaluated between control and diseased eye, the OCTA sensitivity can be compromised. A recent study revealed two differential A–V features, i.e. artery vein ratio of blood vessel caliber and tortuosity to improve the OCTA performance for DR classification,[41] and predominant BVD and BVT distortions were observed in venous system in case of SCR.[40]

Quantitative analysis of choroidal vasculature has been explored predominantly for AMD assessment.[61,158] Dry AMD is generally characterized by decreased foveal choroidal blood flow and increased drusen and GA. In case of wet AMD, CNVs are the most commonly used biomarkers for quantitative OCTA analysis.[61,165] Jia *et al.*[15] first presented a study focused on using OCTA to detect and classify the types of CNVs. This study reported that the en-face angiograms showed decreased choroidal flow adjacent to the CNV in all cases. Cross-sectional angiograms were able to visualize location and classify the CNV as type I and type II. In following studies,[57] the researchers analyzed artifact removal algorithms, slab subtraction, and PR-OCTA for quantification of CNV area and connectivity. Miller *et al.*[159] compared CNV using SS and SD-OCTA, and reported statistically significant differences between SS-OCTA and SD-OCTA measured lesion areas. SS-OCTA showed larger lesion area when compared to SD-OCTA in both 3×3 mm^2 and 6×6 mm^2, with larger differences reported in the 6×6 mm^2. Similarly, Zhang *et al.*[56] reported that SS-OCTA allowed for deeper light penetration into the choroid. Another parameter that has been studied for AMD is FD. Al-Sheikh *et al.*[30] studied CNV lesions in AMD pre- and post-treatment of anti-vascular endothelial growth

Table 1. Summary of quantitative OCTA features.

Features	Applications	Clinical OCTA with built-in software	Clinical OCTA with custom software	Custom OCTA
BVD	To quantify blood vessel density and identifies ischemic regions in DR, SCR, AMD, glaucoma, VO, etc.	21, 29, 47, 50, 66–77	22, 24, 25, 30 –33, 35–39, 41, 42, 45, 65, 72, 74, 78–112	113, 114
BVC	To quantify blood vessel width, dilation, or shrinkage in DR, SCR, etc.	115	22, 35, 37–41, 43, 85, 87–89, 95, 96, 99, 102, 108, 110, 116, 117	113, 114, 118
BVT	To quantify blood vessel tortuosity due to change in morphology in DR, VO, SCR, etc.	119	26, 33, 35, 38–41, 98, 101, 117, 120–123	114
VPI	To quantify changes in the perimeter of blood vessels in DR, VO, SCR, etc.	–	22, 35, 38, 39, 42, 95, 96, 102, 110, 112	–
FAZ-A	To quantify changes in foveal area in DR, DME, SCR, etc.	21, 26–29, 34, 44, 47, 50, 66–71,73, 75, 77, 115, 119, 124–137	24, 26, 33, 35, 38, 39, 43–46, 48, 72, 74, 78, 79, 81, 89–94, 98, 100, 101, 103, 105, 107, 108, 110, 119, 132, 138–148	–
FAZ-CI	To quantify changes in foveal complexity in DR, DME, VO, AMD and SCR.	47, 48, 66, 67, 70, 72, 136	46, 78, 79, 89, 90, 92, 110, 132, 139, 142 –144	–
VCI	To quantify changes in retinal vascular complexity in DR, SCR, etc.	–	30, 32, 36, 37, 49, 65, 79–88, 90, 102, 104, 149, 150–154	–
BPA	To quantify changes in vascular bifurcation in DR, etc.	–	52	–
A–V analysis	To achieve differential artery and vein analysis in DR, SCR, etc.	–	40, 41, 116	54
Flow analysis	To quantify changes in blood flow in DR, GA, AMD, etc.	21, 125	24, 55–57, 106, 109, 138, 155, 156	15, 61, 157
CNV analysis	To quantify neovascularization activity in AMD, etc.	–	30, 57, 63–65, 82, 117, 149, 151, 156, 158–160	15, 61, 159

AMD: age-related macular degeneration; A–V: artery–vein; AVR: artery–vein ratio; BPA: branchpoint analysis; BVC: blood vessel caliber; BVD: blood vessel density; BVT: blood vessel tortuosity; CI: contour irregularity; CNV: choroidal neovascular; DME: diabetic macular edema; DR: diabetic retinopathy; FAZ: foveal avascular zone; FAZ-A: fovea avascular zone area; FAZ-CI: FAZ contour irregularity; FD: fractal dimension; GA: geographic atrophy; LAC: lacunarity; OCTA: OCT angiography; SCR: sickle cell retinopathy; VCI: vessel complexity index; VO: vein occlusion; VPI: vessel perimeter index.

factors, and reported a lower FD in the inner part of the lesion after treatment.

Quantitative OCTA opens a unique opportunity to enable computer-aided disease detection and AI classification of different eye diseases. Machine learning techniques have been explored to segment microvasculature,[166] nonperfusion areas,[167] optical nerve head.[168] A support vector machine (SVM) classifier was recently demonstrated for supervised machine learning based OCTA classification of SCR[35] and DR.[39] Six OCTA features, i.e. BVD, BVC, BVT, VPI, FAZ-A, and FAZ-CI, were used to train the SVM classifier for identifying control, mild, and severe SCR subjects.[35] The SVM was able to identify control versus disease and mild versus severe SCR with 100 and 97% accuracies, respectively. A similar approach was also adopted for OCTA classification of NPDR.[39] The study demonstrated 94.41% accuracy for control versus disease (i.e. NPDR) and 92.96% accuracy for control versus mild NPDR classification. The control versus mild NPDR classification was important for early DR detection. In another study, three OCTA features, i.e. BVD, BVC, and FAZ-A, were used for automated classification of NPDR with 94.3% accuracy.[108] Supervised machine learning was also recently validated for multiple-task classification to differentiate control, SCR and DR from each other.[20] In principle, both supervised and unsupervised machine learning techniques can be considered for AI classification of OCTA images. However, the limited size of currently available database is a major challenging factor for deep learning-based AI classification of OCTA. With the increasing OCTA applications in ophthalmology to expand the available OCTA datasets, we anticipate that deep learning-based classification, which has been well established for fundus image classification, will play an important role to enable automated OCTA detection and classification of eye conditions. Alternatively, transfer learning-based technology[169] may find valuable application in the near future to foster the deep learning OCTA classification of eye diseases.

Authors' contributions: Original draft preparation: XY, MNA, DL; manuscript review and editing: XY and DT; project supervision: XY.

DECLARATION OF CONFLICTING INTERESTS

The author(s) declared no potential conflicts of interest with respect to the research, authorship, and/or publication of this article.

FUNDING

This research was supported in part by NIH grants R01 EY030101, R01EY029673, R01 EY023522, P30 EY001792; by unrestricted grant from Research to Prevent Blindness; by Richard and Loan Hill endowment.

ORCID IDS

Minhaj N Alam https://orcid.org/0000-0003-3095-2232
David Le https://orcid.org/0000-0003-3772-1875

REFERENCES

1. Sharp PF, Manivannan A. The scanning laser ophthalmoscope. *Phys Med Biol* 1997;**42**:951–66
2. Kobayashi K, Asakura T. Imaging techniques and applications of the scanning laser ophthalmoscope. *Opt Eng* 1995;**34**:717–26
3. Liang JZ, Williams DR, Miller DT. High resolution imaging of the living human retina with adaptive optics. *Invest Ophthalmol Vis Sci* 1997;**38**:55
4. Burns SA, Elsner AE, Sapoznik KA, Warner RL, Gast TJ. Adaptive optics imaging of the human retina. *Prog Retin Eye Res* 2019;**68**:1–30
5. Paques M, Meimon S, Rossant F, Rosenbaum D, Mrejen S, Sennlaub F, Grieve K. Adaptive optics ophthalmoscopy: application to age-related macular degeneration and vascular diseases. *Prog Retin Eye Res* 2018;**66**:1–16
6. Banda HK, Shah GK, Blinder KJ. Applications of fundus autofluorescence and widefield angiography in clinical practice. *Can J Ophthalmol* 2019;**54**:11–19
7. Mehta S. Fundus fluorescein angiography of choroidal tubercles: case reports and review of literature. *Indian J Ophthalmol* 2006;**54**:273–5
8. Huang D, Swanson EA, Lin CP, Schuman JS, Stinson WG, Chang W, Hee MR, Flotte T, Gregory K, Puliafito CA, Fujimoto JG. Optical coherence tomography. *Science* 1991;**254**:1178–81
9. Mailankody P, Lenka A, Pal PK. The role of optical coherence tomography in Parkinsonism: a critical review. *J Neurol Sci* 2019;**403**:67–74
10. Ruia S, Saxena S, Gemmy Cheung CM, Gilhotra JS, Lai TY. Spectral domain optical coherence tomography features and classification systems for diabetic macular edema: a review. *Asia Pac J Ophthalmol* 2016;**5**:360–7
11. Sohrab MA, Fawzi AA. Review of en-face choroidal imaging using spectral-domain optical coherence tomography. *Med Hypothesis Discov Innov Ophthalmol* 2013;**2**:69–73
12. Gao SS, Jia Y, Zhang M, Su JP, Liu G, Hwang TS, Bailey ST, Huang D. Optical coherence tomography angiography. *Invest Ophthalmol Vis Sci* 2016;**57**:OCT27–36
13. Zhang A, Zhang Q, Chen CL, Wang RK. Methods and algorithms for optical coherence tomography-based angiography: a review and comparison. *J Biomed Opt* 2015;**20**:100901
14. Bandello F, Corbelli E, Carnevali A, Pierro L, Querques G. Optical coherence tomography angiography of diabetic retinopathy. *Dev Ophthalmol* 2016;**56**:107–12
15. Jia Y, Bailey ST, Wilson DJ, Tan O, Klein ML, Flaxel CJ, Potsaid B, Liu JJ, Lu CD, Kraus MF. Quantitative optical coherence tomography angiography of choroidal neovascularization in age-related macular degeneration. *Ophthalmology* 2014;**121**:1435–44
16. Dastiridou A, Chopra V. Potential applications of optical coherence tomography angiography in glaucoma. *Curr Opin Ophthalmol* 2018;**29**:226–33
17. Bojikian KD, Chen PP, Wen JC. Optical coherence tomography angiography in glaucoma. *Curr Opin Ophthalmol* 2019;**30**:110–16
18. Leitao Guerra RL, Leitao Guerra CL, Bastos MG, de Oliveira AHP, Salles C. Sickle cell retinopathy: what we now understand using optical coherence tomography angiography. A systematic review. *Blood Rev* 2019;**35**:32–42
19. Faatz H, Farecki ML, Rothaus K, Gunnemann F, Gutfleisch M, Lommatzsch A, Pauleikhoff D. Optical coherence tomography angiography of types 1 and 2 choroidal neovascularization in age-related macular degeneration during anti-VEGF therapy: evaluation of a new quantitative method. *Eye* 2019;**33**:1466–1471
20. Alam M, Le D, Lim JI, Chan RVP, Yao XC. Supervised machine learning based multi-task artificial intelligence classification of retinopathies. *J Clin Med* 2019;**8**:872
21. Chao S-C, Yang S-J, Chen H-C, Sun C-C, Liu C-H, Lee C-Y. Early macular angiography among patients with glaucoma, ocular hypertension, and normal subjects. *J Ophthalmol* 2019; **2019**:7419470
22. Lin T-C, Gogte P, Palejwala N, Shahidzadeh A, Itty S, Humayun MS, Moshfeghi AA, Ameri H, Chu Z, Wang RK. Quantitative spectral-domain optical coherence tomography angiography (OCTA) of diabetic retinopathy (DR) severity. *Invest Ophthalmol Vis Sci* 2017;**58**:1653–1653
23. Camino A, Zhang M, Liu L, Wang J, Jia Y, Huang D. Enhanced quantification of retinal perfusion by improved discrimination of blood flow from bulk motion signal in OCTA. *Transl Vis Sci Technol* 2018;**7**:20–20
24. Nesper PL, Roberts PK, Onishi AC, Chai H, Liu L, Jampol LM, Fawzi AA. Quantifying microvascular abnormalities with increasing severity of diabetic retinopathy using optical coherence tomography angiography. *Invest Ophthalmol Vis Sci* 2017;**58**:BIO307–15
25. Pedinielli A, Bonnin S, Sanharawi ME, Mane V, Erginay A, Couturier A, Tadayoni R. Three different optical coherence tomography angiography measurement methods for assessing capillary density changes in diabetic retinopathy. *Ophthalmic Surg Lasers Imaging Retina* 2017;**48**:378–84
26. Mastropasqua R, Toto L, Mastropasqua A, Aloia R, De Nicola C, Mattei PA, Di Marzio G, Di Nicola M, Di Antonio L. Foveal avascular zone area and parafoveal vessel density measurements in different stages of diabetic retinopathy by optical coherence tomography angiography. *Int J Ophthalmol* 2017;**10**:1545
27. Falavarjani KG, Scott AW, Wang K, Han IC, Chen X, Klufas M, Hubschman J-P, Schwartz SD, Sadda SR, Sarraf D. Correlation of multimodal imaging in sickle cell retinopathy. *Retina* 2016;**36**:S111–17
28. Minvielle W, Caillaux V, Cohen SY, Chasset F, Zambrowski O, Miere A, Souied EH. Macular microangiopathy in sickle cell disease using optical coherence tomography angiography. *Am J Ophthalmol* 2016;**164**:137–44.e1
29. Jhaj G, Glazman S, Shrier EM, Bodis-Wollner I. Non-exudative age-related macular degeneration foveal avascular zone area, foveal vessel density, and ganglion cell complex thickness. *Invest Ophthalmol Vis Sci* 2017;**58**:36–36
30. Al-Sheikh M, Iafe NA, Phasukkijwatana N, Sadda SR, Sarraf D. Biomarkers of neovascular activity in age-related macular degeneration using optical coherence tomography angiography. *Retina* 2018;**38**:220–30
31. Liu L, Jia Y, Takusagawa HL, Pechauer AD, Edmunds B, Lombardi L, Davis E, Morrison JC, Huang D. Optical coherence tomography angiography of the peripapillary retina in glaucoma. *JAMA Ophthalmol* 2015;**133**:1045–52
32. Richter GM, Chang R, Situ B, Chu Z, Burkemper B, Reznik A, Bedrood S, Kashani AH, Varma R, Wang RK. Diagnostic performance of macular versus peripapillary vessel parameters by optical coherence tomography angiography for glaucoma. *Transl Vis Sci Technol* 2018;**7**:21
33. Adhi M, Filho MA, Louzada RN, Kuehlewein L, de Carlo TE, Baumal CR, Witkin AJ, Sadda SR, Sarraf D, Reichel E, Duker JS, Waheed NK. Retinal capillary network and foveal avascular zone in eyes with vein occlusion and fellow eyes analyzed with optical coherence tomography angiography. *Invest Ophthalmol Vis Sci* 2016;**57**:OCT486–94
34. Winegarner A, Wakabayashi T, Fukushima Y, Sato T, Hara-Ueno C, Busch C, Nishiyama I, Shiraki N, Sayanagi K, Nishida K, Sakaguchi H, Nishida K. Changes in retinal microvasculature and visual acuity after antivascular endothelial growth factor therapy in retinal vein occlusion. *Invest Ophthalmol Vis Sci* 2018;**59**:2708–16

35. Alam M, Thapa D, Lim JI, Cao D, Yao X. Computer-aided classification of sickle cell retinopathy using quantitative features in optical coherence tomography angiography. *Biomed Opt Express* 2017;**8**:4206–16
36. Richter GM, Madi I, Chu Z, Burkemper B, Chang R, Zaman A, Sylvester B, Reznik A, Kashani A, Wang RK, Varma R. Structural and functional associations of macular microcirculation in the ganglion cell-inner plexiform layer in glaucoma using optical coherence tomography angiography. *J Glaucoma* 2018;**27**:281–90
37. Akagi T, Uji A, Huang AS, Weinreb RN, Yamada T, Miyata M, Kameda T, Ikeda HO, Tsujikawa A. Conjunctival and intrascleral vasculatures assessed using anterior segment optical coherence tomography angiography in normal eyes. *Am J Ophthalmol* 2018;**196**:1–9
38. Alam M, Thapa D, Lim JI, Cao D, Yao X. Quantitative characteristics of sickle cell retinopathy in optical coherence tomography angiography. *Biomed Opt Express* 2017;**8**:1741–53
39. Alam M, Zhang Y, Lim JI, Chan RV, Yang M, Yao X. Quantitative optical coherence tomography angiography features for objective classification and staging of diabetic retinopathy. *Retina* 2019
40. Alam M, Lim JI, Toslak D, Yao X. Differential artery–vein analysis improves the performance of OCTA staging of sickle cell retinopathy. *Transl Vis Sci Technol* 2019;**8**:3–3
41. Alam M, Toslak D, Lim JI, Yao X. Color fundus image guided artery-vein differentiation in optical coherence tomography angiography. *Invest Ophthalmol Vis Sci* 2018;**59**:4953–62
42. Ye H, Zheng C, Lan X, Zhao L, Qiao T, Li X, Zhang Y. Evaluation of retinal vasculature before and after treatment of children with obstructive sleep apnea-hypopnea syndrome by optical coherence tomography angiography. *Graefes Arch Clin Exp Ophthalmol* 2019;**257**:543–48
43. Chu Z, Lin J, Gao C, Xin C, Zhang Q, Chen C-L, Roisman L, Gregori G, Rosenfeld PJ, Wang RK. Quantitative assessment of the retinal microvasculature using optical coherence tomography angiography. *J Biomed Opt* 2016;**13**:1–13
44. Durbin MK, An L, Shemonski ND, Soares M, Santos T, Lopes M, Neves C, Cunha-Vaz J. Quantification of retinal microvascular density in optical coherence tomographic angiography images in diabetic retinopathy. *JAMA Ophthalmol* 2017;**135**:370–76
45. Falavarjani KG, Iafe NA, Hubschman J-P, Tsui I, Sadda SR, Sarraf D. Optical coherence tomography angiography analysis of the foveal avascular zone and macular vessel density after anti-VEGF therapy in eyes with diabetic macular edema and retinal vein occlusion. *Invest Ophthalmol Vis Sci* 2017;**58**:30–34
46. Krawitz BD, Mo S, Geyman LS, Agemy SA, Scripsema NK, Garcia PM, Chui TY, Rosen RB. Acircularity index and axis ratio of the foveal avascular zone in diabetic eyes and healthy controls measured by optical coherence tomography angiography. *Vision Res* 2017;**139**:177–86
47. Li Z, Alzogool M, Xiao J, Zhang S, Zeng P, Lan Y. Optical coherence tomography angiography findings of neurovascular changes in type 2 diabetes mellitus patients without clinical diabetic retinopathy. *Acta Diabetol* 2018;**55**:1075–82
48. Philip S, Najafi A, Tantraworasin A, Chui TYP, Rosen RB, Ritch R. Macula vessel density and foveal avascular zone parameters in exfoliation glaucoma compared to primary open-angle glaucoma. *Invest Ophthalmol Vis Sci* 2019;**60**:1244–53
49. Zahid S, Dolz-Marco R, Freund KB, Balaratnasingam C, Dansingani K, Gilani F, Mehta N, Young E, Klifto MR, Chae B, Yannuzzi LA, Young JA. Fractal dimensional analysis of optical coherence tomography angiography in eyes with diabetic retinopathy. *Invest Ophthalmol Vis Sci* 2016;**57**:4940–47
50. Cabral D, Coscas F, Glacet-Bernard A, Pereira T, Geraldes C, Cachado F, Papoila A, Coscas G, Souied E. Biomarkers of peripheral nonperfusion in retinal venous occlusions using optical coherence tomography angiography. *Transl Vis Sci Technol* 2019;**8**:7–7
51. Murray CD. The physiological principle of minimum work: I. The vascular system and the cost of blood volume. *Proc Natl Acad Sci USA* 1926;**12**:207–14
52. Le D, Alam M, Miao BA, Lim JI, Yao X. Fully automated geometric feature analysis in optical coherence tomography angiography for objective classification of diabetic retinopathy. *Biomed Opt Express* 2019;**10**:2493–503
53. Alam M, Toslak D, Lim JI, Yao X. OCT feature analysis guided artery-vein differentiation in OCTA. *Biomed Opt Express* 2019;**10**:2055–66
54. Son T, Alam M, Kim T-H, Liu C, Toslak D, Yao X. Near infrared oximetry-guided artery–vein classification in optical coherence tomography angiography. *Exp Biol Med* 2019; **244**:813–818
55. Wang X, Jia Y, Spain R, Potsaid B, Liu JJ, Baumann B, Hornegger J, Fujimoto JG, Wu Q, Huang D. Optical coherence tomography angiography of optic nerve head and parafovea in multiple sclerosis. *Br J Ophthalmol* 2014;**98**:1368–73
56. Zhang Q, Zheng F, Motulsky EH, Gregori G, Chu Z, Chen C-L, Li C, de Sisternes L, Durbin M, Rosenfeld PJ, Wang RK. A novel strategy for quantifying choriocapillaris flow voids using swept-source OCT angiography quantifying choriocapillaris flow voids using SS-OCTA. *Invest Ophthalmol Vis Sci* 2018;**59**:203–11
57. Patel R, Wang J, Campbell JP, Kiang L, Lauer A, Flaxel C, Hwang T, Lujan B, Huang D, Bailey ST. Classification of choroidal neovascularization using projection-resolved optical coherence tomographic angiography. *Invest Ophthalmol Vis Sci* 2018;**59**:4285–91
58. Baumann B, Potsaid B, Kraus MF, Liu JJ, Huang D, Hornegger J, Cable AE, Duker JS, Fujimoto JG. Total retinal blood flow measurement with ultrahigh speed swept source/Fourier domain OCT. *Biomed Opt Express* 2011;**2**:1539–52
59. Pechauer AD, Jia Y, Liu L, Gao SS, Jiang C, Huang D. Optical coherence tomography angiography of peripapillary retinal blood flow response to hyperoxia OCT angiography of retinal blood flow during hyperoxia. *Invest Ophthalmol Vis Sci* 2015;**56**:3287–91
60. Tan O, Liu G, Liang L, Gao SS, Pechauer AD, Jia Y, Huang D. En face Doppler total retinal blood flow measurement with 70 kHz spectral optical coherence tomography. *J Biomed Opt* 2015;**20**:066004.
61. Moult E, Choi W, Waheed NK, Adhi M, Lee B, Lu CD, Jayaraman V, Potsaid B, Rosenfeld PJ, Duker JS, Fujimoto JG. Ultrahigh-speed swept-source OCT angiography in exudative AMD. *Ophthalmic Surg Lasers Imaging Retina* 2014;**45**:496–505
62. Ploner SB, Moult EM, Choi W, Waheed NK, Lee B, Novais EA, Cole ED, Potsaid B, Husvogt L, Schottenhamml J, Maier A, Rosenfeld PJ, Duker JS, Hornegger J, Fujimoto JG. Toward quantitative optical coherence tomography angiography: visualizing blood flow speeds in ocular pathology using variable interscan time analysis. *Retina* 2016;**36**:S118–26
63. Uchida A, Hu M, Babiuch A, Srivastava SK, Singh RP, Kaiser PK, Talcott K, Rachitskaya A, Ehlers JP. Optical coherence tomography angiography characteristics of choroidal neovascularization requiring varied dosing frequencies in treat-and-extend management: an analysis of the AVATAR study. *PLoS One* 2019;**14**:e0218889
64. Carnevali A, Cicinelli MV, Capuano V, Corvi F, Mazzaferro A, Querques L, Scorcia V, Souied EH, Bandello F, Querques G. Optical coherence tomography angiography: a useful tool for diagnosis of treatment-naïve quiescent choroidal neovascularization. *Am J Ophthalmol* 2016;**169**:189–98
65. Coscas F, Cabral D, Pereira T, Geraldes C, Narotamo H, Miere A, Lupidi M, Sellam A, Papoila A, Coscas G. Quantitative optical coherence tomography angiography biomarkers for neovascular age-related macular degeneration in remission. *PLoS One* 2018;**13**:e0205513
66. Lim HB, Kim YW, Kim JM, Jo YJ, Kim JY. The importance of signal strength in quantitative assessment of retinal vessel density using optical coherence tomography angiography. *Sci Rep* 2018;**8**:12897
67. Liu L, Gao J, Bao W, Hu C, Xu Y, Zhao B, Zheng J, Fan L, Sun Y. Analysis of foveal microvascular abnormalities in diabetic retinopathy using optical coherence tomography angiography with projection artifact removal. *J Ophthalmol* 2018; **2018**:3926745
68. Yu S, Frueh BE, Steinmair D, Ebneter A, Wolf S, Zinkernagel MS, Munk MR. Cataract significantly influences quantitative measurements on swept-source optical coherence tomography angiography imaging. *PLoS One* 2018;**13**:e0204501

69. Corvi F, Pellegrini M, Erba S, Cozzi M, Staurenghi G, Giani A. Reproducibility of vessel density, fractal dimension, and foveal avascular zone using 7 different optical coherence tomography angiography devices. *Am J Ophthalmol* 2018;**186**:25–31
70. Tian M, Tappeiner C, Zinkernagel MS, Wolf S, Munk MR. Swept-source optical coherence tomography angiography reveals vascular changes in intermediate uveitis. *Acta Ophthalmol* 2019;97:e785–e791
71. Lavia C, Bonnin S, Maule M, Erginay A, Tadayoni R, Gaudric A. Vessel density of superficial, intermediate, and deep capillary plexuses using optical coherence tomography angiography. *Retina* 2019;**39**:247
72. Li T, Jia Y, Wang S, Wang A, Gao L, Yang C, Zou H. Retinal microvascular abnormalities in children with type 1 diabetes mellitus without visual impairment or diabetic retinopathy. *Invest Ophthalmol Vis Sci* 2019;**60**:990–98
73. Cao D, Yang D, Huang Z, Zeng Y, Wang J, Hu Y, Zhang L. Optical coherence tomography angiography discerns preclinical diabetic retinopathy in eyes of patients with type 2 diabetes without clinical diabetic retinopathy. *Acta Diabetol* 2018;**55**:469–77
74. Garrity ST, Iafe NA, Phasukkijwatana N, Chen X, Sarraf D. Quantitative analysis of three distinct retinal capillary plexuses in healthy eyes using optical coherence tomography angiography. *Invest Ophthalmol Vis Sci* 2017;**58**:5548–55
75. Fujiwara A, Mengxuan L, Morizane Y, Hosogi M, Kimura S, Hosokawa M, Shiode Y, Masayuki H, Doi S, Toshima S. Interocular symmetry of foveal avascular zone area in healthy eyes: an examination using swept-source optical coherence tomography angiography. *Invest Ophthalmol Vis Sci* 2018;**59**:2882–2882
76. Eastline M, Munk MR, Wolf S, Schaal KB, Ebneter A, Tian M, Giannakaki-Zimmermann H, Zinkernagel MS. Repeatability of wide-field optical coherence tomography angiography in normal retina. *Transl Vis Sci Technol* 2019;**8**:6 [31106033
77. Lutsenko N, Rudycheva O, Isakova O. Assessing OCTA changes in morphology and structure of retinal microvascular bed in patients with exudative AMD. *Journal of Ophthalmology (Ukraine)* 2019;**2**:2–2
78. Kwon J, Choi J, Shin JW, Lee J, Kook MS. Alterations of the foveal avascular zone measured by optical coherence tomography angiography in glaucoma patients with central visual field defects. *Invest Ophthalmol Vis Sci* 2017;**58**:1637–45
79. Ashraf M, Nesper PL, Jampol LM, Yu F, Fawzi AA. Statistical model of optical coherence tomography angiography parameters that correlate with severity of diabetic retinopathy. *Invest Ophthalmol Vis Sci* 2018;**59**:4292–98
80. Agarwal A, Aggarwal K, Akella M, Agrawal R, Khandelwal N, Bansal R, Singh R, Gupta V. Fractal dimension and optical coherence tomography angiography features of the central macula after repair of rhegmatogenous retinal detachments. *Retina* 2018;**39**:2167–2177
81. Kim SV, Semoun O, Pedinielli A, Jung C, Miere A, Souied EH. Optical coherence tomography angiography quantitative assessment of exercise-induced variations in retinal vascular plexa of healthy subjects. *Invest Ophthalmol Vis Sci* 2019;**60**:1412–19
82. Murakawa S, Maruko I, Kawano T, Hasegawa T, Iida T. Choroidal neovascularization imaging using multiple en face optical coherence tomography angiography image averaging. *Graefes Arch Clin Exp Ophthalmol* 2019;**257**:1119–1125
83. Dave VP, Pappuru RR, Gindra R, Ananthakrishnan A, Modi S, Trivedi M, Harikumar P. OCT angiography fractal analysis-based quantification of macular vascular density in BRVO eyes. *Can J Ophthalmol* 2018;**50**:297–300
84. Hirano T, Kitahara J, Toriyama Y, Kasamatsu H, Murata T, Sadda S. Quantifying vascular density and morphology using different swept-source optical coherence tomography angiographic scan patterns in diabetic retinopathy. *Br J Ophthalmol* 2019;**103**:216–21
85. Koulisis N, Kim AY, Chu Z, Shahidzadeh A, Burkemper B, de Koo LCO, Moshfeghi AA, Ameri H, Puliafito CA, Isozaki VL. Quantitative microvascular analysis of retinal venous occlusions by spectral domain optical coherence tomography angiography. *PLoS One* 2017;**12**:e0176404
86. Al-Sheikh M, Phasukkijwatana N, Dolz-Marco R, Rahimi M, Iafe NA, Freund KB, Sadda SR, Sarraf D. Quantitative OCT angiography of the retinal microvasculature and the choriocapillaris in myopic eyes. *Invest Ophthalmol Vis Sci* 2017;**58**:2063–69
87. Kim AY, Rodger DC, Shahidzadeh A, Chu Z, Koulisis N, Burkemper B, Jiang X, Pepple KL, Wang RK, Puliafito CA. Quantifying retinal microvascular changes in uveitis using spectral-domain optical coherence tomography angiography. *Am J Ophthalmol* 2016;**171**:101–12
88. Kim AY, Chu Z, Shahidzadeh A, Wang RK, Puliafito CA, Kashani AH. Quantifying microvascular density and morphology in diabetic retinopathy using spectral-domain optical coherence tomography angiography. *Invest Ophth Vis Sci* 2016;**57**:OCT362–70
89. Rosen RB, Krawitz B, Mo S, Geyman L, Phillips E, Carroll J, Weitz R, Chui TYP. Age-Related variations in foveal avascular zone geometry and vessel density-an optical coherence tomography angiography (OCTA) study x. *Invest Ophthalmol Vis Sci* 2016;**57**:5501–5501
90. Fang D, Tang FY, Huang H, Cheung CY, Chen H. Repeatability, interocular correlation and agreement of quantitative swept-source optical coherence tomography angiography macular metrics in healthy subjects. *Br J Ophthalmol* 2019;**103**:415–20
91. Rabiolo A, Gelormini F, Marchese A, Cicinelli MV, Triolo G, Sacconi R, Querques L, Bandello F, Querques G. Macular perfusion parameters in different angiocube sizes: does the size matter in quantitative optical coherence tomography angiography? *Invest Ophthalmol Vis Sci* 2018;**59**:231–37
92. Mo S, Krawitz B, Efstathiadis E, Geyman L, Weitz R, Chui TY, Carroll J, Dubra A, Rosen RB. Imaging foveal microvasculature: optical coherence tomography angiography versus adaptive optics scanning light ophthalmoscope fluorescein angiography. *Invest Ophthalmol Vis Sci* 2016;**57**:OCT130–40
93. Iafe NA, Phasukkijwatana N, Chen X, Sarraf D. Retinal capillary density and foveal avascular zone area are age-dependent: quantitative analysis using optical coherence tomography angiography. *Invest Ophthalmol Vis Sci* 2016;**57**:5780–87
94. Kwon J, Choi J, Shin JW, Lee J, Kook MS. An optical coherence tomography angiography study of the relationship between foveal avascular zone size and retinal vessel density. *Invest Ophthalmol Vis Sci* 2018;**59**:4143–53
95. Zhang Y, Do B, Mustafi D, Kogachi K, Chu Z, Wang RK, Rodger DC, Rao NA, Kashani AH. Assessing response of retinal microvasculature density and morphology to intra-vitreal dexamethasone implant injections for ocular inflammatory disease with spectral domain optical coherence tomography angiography (SD-OCTA). *Invest Ophthalmol Vis Sci* 2018;**59**:2835–2835
96. Shahidzadeh A, Chen YC, Chu Z, Wang RK, Kashani AH. Correlation of macular thickness with microvascular density and morphology using spectral domain optical coherence tomography angiography (SD-OCTA) among normal subjects. *Invest Ophthalmol Vis Sci* 2018;**59**:2869–2869
97. Falavarjani KG, Tian JJ, Akil H, Garcia GA, Sadda SR, Sadun AA. Swept-source optical coherence tomography angiography of the optic disk in optic neuropathy. *Retina* 2016;**36**:S168–77
98. Talisa E, Chin AT, Bonini Filho MA, Adhi M, Branchini L, Salz DA, Baumal CR, Crawford C, Reichel E, Witkin AJ, Duker JS, Waheed NK. Detection of microvascular changes in eyes of patients with diabetes but not clinical diabetic retinopathy using optical coherence tomography angiography. *Retina* 2015;**35**:2364–70
99. Lei J, Yi E, Suo Y, Chen C, Xu X, Ding W, Abdelfattah NS, Fan X, Lu H. Distinctive analysis of macular superficial capillaries and large vessels using optical coherence tomographic angiography in healthy and diabetic eyes. *Invest Ophthalmol Vis Sci* 2018;**59**:1937–43
100. Kaizu Y, Nakao S, Yoshida S, Hayami T, Arima M, Yamaguchi M, Wada I, Hisatomi T, Ikeda Y, Ishibashi T. Optical coherence tomography angiography reveals spatial bias of macular capillary dropout in diabetic retinopathy. *Invest Ophthalmol Vis Sci* 2017;**58**:4889–97
101. Kim J-A, Kim T-W, Lee EJ, Girard MJ, Mari JM. Microvascular changes in peripapillary and optic nerve head tissues after trabeculectomy in primary open-angle glaucoma. *Invest Ophthalmol Vis Sci* 2018;**59**:4614–21
102. Muraoka Y, Uji A, Ishikura M, Iida Y, Ooto S, Tsujikawa A. Segmentation of the four-layered retinal vasculature using

high-resolution optical coherence tomography angiography reveals the microcirculation unit. *Invest Ophthalmol Vis Sci* 2018;**59**:5847–53
103. Anegondi N, Kshirsagar A, Mochi TB, Roy AS. Quantitative comparison of retinal vascular features in optical coherence tomography angiography images from three different devices. *Ophthalmic Surg Lasers Imaging Retina* 2018;**49**:488–96
104. Gadde SG, Anegondi N, Bhanushali D, Chidambara L, Yadav NK, Khurana A, Roy AS. Quantification of vessel density in retinal optical coherence tomography angiography images using local fractal dimension. *Invest Ophthalmol Vis Sci* 2016;**57**:246–52
105. Wang Q, Chan S, Yang JY, You B, Wang YX, Jonas JB, Wei WB. Vascular density in retina and choriocapillaris as measured by optical coherence tomography angiography. *Am J Ophthalmol* 2016;**168**:95–109
106. Onishi AC, Nesper PL, Roberts PK, Moharram GA, Chai H, Liu L, Jampol LM, Fawzi AA. Importance of considering the middle capillary plexus on OCT angiography in diabetic retinopathy. *Invest Ophthalmol Vis Sci* 2018;**59**:2167–76
107. Hwang TS, Gao SS, Liu L, Lauer AK, Bailey ST, Flaxel CJ, Wilson DJ, Huang D, Jia Y. Automated quantification of capillary nonperfusion using optical coherence tomography angiography in diabetic retinopathy. *JAMA Ophthalmol* 2016;**134**:367–73
108. Sandhu HS, Eladawi N, Elmogy M, Keynton R, Helmy O, Schaal S, El-Baz A. Automated diabetic retinopathy detection using optical coherence tomography angiography: a pilot study. *Br J Ophthalmol* 2018;**102**:1564–69
109. Jia Y, Bailey ST, Hwang TS, McClintic SM, Gao SS, Pennesi ME, Flaxel CJ, Lauer AK, Wilson DJ, Hornegger J. Quantitative optical coherence tomography angiography of vascular abnormalities in the living human eye. *Proc Natl Acad Sci USA* 2015;**112**:E2395–402
110. Hsieh Y-T, Alam MN, Le D, Hsiao C-C, Yang C-H, Chao D, Yao X. Optical coherence tomography angiography biomarkers for predicting visual outcomes after ranibizumab treatment for diabetic macular edema. *Ophthalmol Retina* 2019
111. Skalet A, Liu L, Binder C, Miller A, Wang J, Wilson D, Crilly R, Thomas C, Hung A, Huang D, Jia Y. Quantitative optical coherence tomography angiography for evaluation of peripapillary retinal capillary circulation after plaque brachytherapy for uveal melanoma. *Ophthalmol Retina* 2018;**2**:244–50
112. Chu Z, Lin J, Gao C, Xin C, Zhang Q, Chen C-L, Roisman L, Gregori G, Rosenfeld PJ, Wang RK. Quantitative assessment of the retinal microvasculature using optical coherence tomography angiography. *J Biomed Opt* 2016;**21**:066008.
113. Kim T-H, Son T, Lu Y, Alam M, Yao X. Comparative optical coherence tomography angiography of Wild-Type and rd10 mouse retinas. *Transl Vis Sci Technol* 2018;**7**:42.
114. Kim Y, Hong HK, Park JR, Choi W, Woo SJ, Park KH, Oh W-Y. Oxygen-induced retinopathy and choroidopathy: in vivo longitudinal observation of vascular changes using OCTA. *Invest Ophthalmol Vis Sci* 2018;**59**:3932–42
115. Inooka D, Ueno S, Kominami T, Sayo A, Okado S, Ito Y, Terasaki H. Quantification of macular microvascular changes in patients with retinitis pigmentosa using optical coherence tomography angiography. *Invest Ophthalmol Vis Sci* 2018;**59**:433–38
116. Arthur E, Elsner AE, Sapoznik KA, Papay JA, Muller MS, Burns SA. Distances from capillaries to arterioles or venules measured using OCTA and AOSLO. *Invest Ophthalmol Vis Sci* 2019;**60**:1833–44
117. Brunner M, Romano V, Steger B, Vinciguerra R, Lawman S, Williams B, Hicks N, Czanner G, Zheng Y, Willoughby CE. Imaging of corneal neovascularization: optical coherence tomography angiography and fluorescence angiography. *Invest Ophthalmol Vis Sci* 2018;**59**:1263–69
118. Hosseinaee Z, Tan B, Martinez A, Bizheva KK. Comparative study of optical coherence tomography angiography and phase-resolved Doppler optical coherence tomography for measurement of retinal blood vessels caliber. *Transl Vis Sci Technol* 2018;**7**:18
119. Vujosevic S, Muraca A, Alkabes M, Villani E, Cavarzeran F, Rossetti L, De Cilla S. Early microvascular and neural changes in patients with type 1 and type 2 diabetes mellitus without clinical signs of diabetic retinopathy. *Retina* 2019;**39**:435–45
120. Chu S, Nesper PL, Soetikno BT, Bakri SJ, Fawzi AA. Projection-resolved OCT angiography of microvascular changes in paracentral acute middle maculopathy and acute macular neuroretinopathy. *Invest Ophthalmol Vis Sci* 2018;**59**:2913–22
121. Dansingani KK, Freund KB. Optical coherence tomography angiography reveals mature, tangled vascular networks in eyes with neovascular age-related macular degeneration showing resistance to geographic atrophy. *Ophthalmic Surg Lasers Imaging Retina* 2015;**46**:907–12
122. Saraf SS, Tyring AJ, Chen C-L, Le TP, Kalina RE, Wang R, Chao JR. Familial retinal arteriolar tortuosity and quantification of vascular tortuosity using swept-source optical coherence tomography angiography. *Am J Ophthalmol Case Rep* 2019;**14**:74–78
123. Khansari MM, O'Neill W, Lim J, Shahidi M. Method For quantitative assessment of retinal vessel tortuosity in optical coherence tomography angiography applied to sickle cell retinopathy. *Biomed Opt Express* 2017;**8**:3796–806
124. Samara WA, Shahlaee A, Sridhar J, Khan MA, Ho AC, Hsu J. Quantitative optical coherence tomography angiography features and visual function in eyes with branch retinal vein occlusion. *Am J Ophthalmol* 2016;**166**:76–83
125. Bulut M, Kurtuluş F, Gözkaya O, Erol MK, Cengiz A, Akıdan M, Yaman A. Evaluation of optical coherence tomography angiographic findings in Alzheimer's type dementia. *Br J Ophthalmol* 2018;**102**:233–37
126. Chang MY, Phasukkijwatana N, Garrity S, Pineles SL, Rahimi M, Sarraf D, Johnston M, Charles A, Arnold AC. Foveal and peripapillary vascular decrement in migraine with aura demonstrated by optical coherence tomography angiography. *Invest Ophthalmol Vis Sci* 2017;**58**:5477–84
127. Conti FF, Qin VL, Rodrigues EB, Sharma S, Rachitskaya AV, Ehlers JP, Singh RP. Choriocapillaris and retinal vascular plexus density of diabetic eyes using split-spectrum amplitude decorrelation spectral-domain optical coherence tomography angiography. *Br J Ophthalmol* 2019;**103**:452–56
128. Dimitrova G, Chihara E, Takahashi H, Amano H, Okazaki K. Quantitative retinal optical coherence tomography angiography in patients with diabetes without diabetic retinopathy. *Invest Ophthalmol Vis Sci* 2017;**58**:190–96
129. Garrity ST, Iafe NA, Phasukkijwatana N, Chen X, Sarraf D. Quantitative analysis of retinal capillary density and foveal avascular zone area using optical coherence tomography angiography of normal eyes. *Invest Ophthalmol Vis Sci* 2017;**58**:3646–3646
130. Goudot MM, Sikorav A, Semoun O, Miere A, Jung C, Courbebaisse B, Srour M, Freiha JG, Souied EH. Parafoveal OCT angiography features in diabetic patients without clinical diabetic retinopathy: a qualitative and quantitative analysis. *J Ophthalmol* 2017;**2017**:8676091
131. Kim K, Kim ES, Yu S-Y. Optical coherence tomography angiography analysis of foveal microvascular changes and inner retinal layer thinning in patients with diabetes. *Br J Ophthalmol* 2018;**102**:1226–31
132. Linderman R, Salmon AE, Strampe M, Russillo M, Khan J, Carroll J. Assessing the accuracy of foveal avascular zone measurements using optical coherence tomography angiography: segmentation and scaling. *Transl Vis Sci Technol* 2017;**6**:16
133. Samara WA, Shahlaee A, Adam MK, Khan MA, Chiang A, Maguire JI, Hsu J, Ho AC. Quantification of diabetic macular ischemia using optical coherence tomography angiography and its relationship with visual acuity. *Ophthalmology* 2017;**124**:235–44
134. Scarinci F, Picconi F, Giorno P, Boccassini B, De Geronimo D, Varano M, Frontoni S, Parravano M. Deep capillary plexus impairment in patients with type 1 diabetes mellitus with no signs of diabetic retinopathy revealed using optical coherence tomography angiography. *Acta Ophthalmol* 2018;**96**:e264–e65
135. Simonett JM, Scarinci F, Picconi F, Giorno P, De Geronimo D, Di Renzo A, Varano M, Frontoni S, Parravano M. Early microvascular retinal changes in optical coherence tomography angiography in patients with type 1 diabetes mellitus. *Acta Ophthalmol* 2017;**95**:e751–55

136. Yeung L, Wu IW, Sun CC, Liu CF, Chen SY, Tseng CH, Lee HC, Lee CC. Early retinal microvascular abnormalities in patients with chronic kidney disease. *Microcirculation* 2019;**26**:e12555
137. Yoon YS, Woo JM, Woo JE, Min JK. Superficial foveal avascular zone area changes before and after idiopathic epiretinal membrane surgery. *Int J Ophthalmol* 2018;**11**:1711
138. Alibhai AY, Moult EM, Shahzad R, Rebhun CB, Moreira-Neto C, McGowan M, Lee D, Lee B, Baumal CR, Witkin AJ. Quantifying microvascular changes using OCT angiography in diabetic eyes without clinical evidence of retinopathy. *Ophthalmol Retina* 2018;**2**:418–27
139. Andrade Romo JS, Linderman RE, Pinhas A, Carroll J, Rosen RB, Chui T. Novel development of parafoveal capillary density deviation mapping using an age-group and eccentricity matched normative OCT angiography database. *Transl Vis Sci Technol* 2019;**8**:1
140. Hwang TS, Jia Y, Gao SS, Bailey ST, Lauer AK, Flaxel CJ, Wilson DJ, Huang D. Optical coherence tomography angiography features of diabetic retinopathy. *Retina* 2015;**35**:2371
141. Kaizu Y, Nakao S, Wada I, Yamaguchi M, Fujiwara K, Yoshida S, Hisatomi T, Ikeda Y, Hayami T, Ishibashi T. Imaging of retinal vascular layers: adaptive optics scanning laser ophthalmoscopy versus optical coherence tomography angiography. *Transl Vis Sci Technol* 2017;**6**:2
142. Krawitz BD, Phillips E, Bavier RD, Mo S, Carroll J, Rosen RB, Chui TY. Parafoveal nonperfusion analysis in diabetic retinopathy using optical coherence tomography angiography. *Transl Vis Sci Technol* 2018;**7**:4–4
143. Lu Y, Simonett JM, Wang J, Zhang M, Hwang T, Hagag AM, Huang D, Li D, Jia Y. Evaluation of automatically quantified foveal avascular zone metrics for diagnosis of diabetic retinopathy using optical coherence tomography angiography. *Invest Ophthalmol Vis Sci* 2018;**59**:2212–21
144. Rosen RB, Andrade Romo JS, Krawitz BD, Mo S, Fawzi AA, Linderman RE, Carroll J, Pinhas A, Chui TYP. Earliest evidence of preclinical diabetic retinopathy revealed using optical coherence tomography angiography perfused capillary density. *Am J Ophthalmol* 2019
145. Samara WA, Say EA, Khoo CT, Higgins TP, Magrath G, Ferenczy S, Shields CL. Correlation of foveal avascular zone size with foveal morphology in normal eyes using optical coherence tomography angiography. *Retina* 2015;**35**:2188–95
146. Schmidt TG, Linderman RE, Strampe MR, Chui TYP, Rosen RB, Carroll J. The utility of frame averaging for automated algorithms in analyzing retinal vascular biomarkers in AngioVue OCTA. *Transl Vis Sci Technol* 2019;**8**:10
147. Takase N, Nozaki M, Kato A, Ozeki H, Yoshida M, Ogura Y. Enlargement of foveal avascular zone in diabetic eyes evaluated by En face optical coherence tomography angiography. *Retina* 2015;**35**:2377–83
148. Tan CS, Lim LW, Chow VS, Chay IW, Tan S, Cheong KX, Tan GT, Sadda SR. Optical coherence tomography angiography evaluation of the parafoveal vasculature and its relationship with ocular factors. *Invest Ophthalmol Vis Sci* 2016;**57**:OCT224–34
149. Anegondi N, Chidambara L, Bhanushali D, Gadde SG, Yadav NK, Sinha Roy A. An automated framework to quantify areas of regional ischemia in retinal vascular diseases with OCT angiography. *J Biophotonics* 2018;**11**:e201600312
150. Sioufi K, Shahlaee A, Say EAT, Ferenczy S, Hsu J, Shields CL. Fractal dimension analysis of parafoveal microvascular anatomy using optical coherence tomography angiography in two machines. *Invest Ophthalmol Vis Sci* 2017;**58**:1674–74
151. Faatz H, Farecki M-L, Rothaus K, Gunnemann F, Gutfleisch M, Lommatzsch A, Pauleikhoff D. Optical coherence tomography angiography of types 1 and 2 choroidal neovascularization in age-related macular degeneration during anti-VEGF therapy: evaluation of a new quantitative method. *Eye* 2019;**33**:1466–1471
152. Ting DSW, Tan GSW, Agrawal R, Yanagi Y, Sie NM, Wong CW, San Yeo IY, Lee SY, Cheung CMG, Wong TY. Optical coherence tomographic angiography in type 2 diabetes and diabetic retinopathy. *JAMA Ophthalmol* 2017;**135**:306–312
153. Chen Q, Ma Q, Wu C, Tan F, Chen F, Wu Q, Zhou R, Zhuang X, Lu F, Qu J. Macular vascular fractal dimension in the deep capillary layer as an early indicator of microvascular loss for retinopathy in type 2 diabetic patients. *Invest Ophthalmol Vis Sci* 2017;**58**:3785–94
154. Bhardwaj S, Tsui E, Zahid S, Young E, Mehta N, Agemy S, Garcia P, Rosen RB, Young JA. Value of fractal analysis of optical coherence tomography angiography in various stages of diabetic retinopathy. *Retina* 2018;**38**:1816–23
155. Spain RI, Liu L, Zhang X, Jia Y, Tan O, Bourdette D, Huang D. Optical coherence tomography angiography enhances the detection of optic nerve damage in multiple sclerosis. *Br J Ophthalmol* 2018;**102**:520–24
156. Ishibazawa A, Nagaoka T, Takahashi A, Omae T, Tani T, Sogawa K, Yokota H, Yoshida A. Optical coherence tomography angiography in diabetic retinopathy: a prospective pilot study. *Am J Ophthalmol* 2015;**160**:35–44.e1
157. Rebhun CB, Moult EM, Novais EA, Moreira-Neto C, Ploner SB, Louzada RN, Lee B, Baumal CR, Fujimoto JG, Duker JS, Waheed NK, Ferrara D. Polypoidal choroidal vasculopathy on swept-source optical coherence tomography angiography with variable interscan time analysis. *Transl Vis Sci Technol* 2017;**6**:4
158. Zheng F, Zhang Q, Motulsky EH, de Oliveira Dias JR, Chen CL, Chu Z, Miller AR, Feuer W, Gregori G, Kubach S, Durbin MK, Wang RK, Rosenfeld PJ. Comparison of neovascular lesion area measurements from different swept-source OCT angiographic scan patterns in age-related macular degeneration. *Invest Ophthalmol Vis Sci* 2017;**58**:5098–104
159. Miller AR, Roisman L, Zhang Q, Zheng F, de Oliveira Dias JR, Yehoshua Z, Schaal KB, Feuer W, Gregori G, Chu Z. Comparison between spectral-domain and swept-source optical coherence tomography angiographic imaging of choroidal neovascularization. *Invest Ophthalmol Vis Sci* 2017;**58**:1499–505
160. Talisa E, Bonini Filho MA, Chin AT, Adhi M, Ferrara D, Baumal CR, Witkin AJ, Reichel E, Duker JS, Waheed NK. Spectral-domain optical coherence tomography angiography of choroidal neovascularization. *Ophthalmology* 2015;**122**:1228–38
161. Chen JL, Zahid S, Alam MN, Yao X, Lim JI. Assessment of quantitative optical coherence tomography angiography parameters in branch retinal vein occlusion and monitoring response to treatment. *Invest Ophthalmol Vis Sci* 2018;**59**:5458–5458
162. Zahid S, Alam MN, Yao X, Lim JI. Quantitative optical coherence tomography angiography parameters in central retinal vein occlusion. *Invest Ophthalmol Vis Sci* 2018;**59**:5427–5427
163. Ouyang Y, Shao Q, Scharf D, Joussen AM, Heussen FM. An easy method to differentiate retinal arteries from veins by spectral domain optical coherence tomography: retrospective, observational case series. *BMC Ophthalmol* 2014;**14**:66
164. Joshi VS, Reinhardt JM, Garvin MK, Abramoff MD. Automated method for identification and artery-venous classification of vessel trees in retinal vessel networks. *PLoS One* 2014;**9**:e88061
165. de Carlo TE, Romano A, Waheed NK, Duker JS. A review of optical coherence tomography angiography (OCTA). *Int J Retina Vitreous* 2015;**1**:5
166. Prentašić P, Heisler M, Mammo Z, Lee S, Merkur A, Navajas E, Beg MF, Šarunic M, Lončarić S. Segmentation of the foveal microvasculature using deep learning networks. *J Biomed Optics* 2016;**21**:075008.
167. Guo Y, Camino A, Wang J, Huang D, Hwang TS, Jia Y. MEDnet, a neural network for automated detection of avascular area in OCT angiography. *Biomed Opt Express* 2018;**9**:5147–58
168. Kasaragod D, Makita S, Hong Y-J, Yasuno Y. Machine-learning based segmentation of the optic nerve head using multi-contrast jones matrix optical coherence tomography with semi-automatic training dataset generation. *Biomed Opt Express* 2018;**9**:3220–43
169. Kermany DS, Goldbaum M, Cai W, Valentim CC, Liang H, Baxter SL, McKeown A, Yang G, Wu X, Yan F. Identifying medical diagnoses and treatable diseases by image-based deep learning. *Cell* 2018;**172**:1122–31.e9